DE-FC26-03NT41965

Separation of Fischer-Tropsch Wax Products from Ultrafine Iron Catalyst Particles

Technical Progress Report

James K. Neathery, Gary Jacobs, Amitava Sarkar, and Burtron H. Davis

Reporting Period
October 1, 2005 to March 30, 2006

The University of Kentucky
Center for Applied Energy Research
2540 Research Park Drive
Lexington, Kentucky 40511-8410

ABSTRACT

The morphological and chemical nature of ultrafine iron catalyst particles (3-5 nm diameters) during activation/FTS was studied by HRTEM, EELS, and Mössbauer spectroscopy. With the progress of FTS, the carbide re-oxidized to magnetite and catalyst activity gradually decreased. The growth of oxide phase continued and average particle size also increased simultaneously. The phase transformation occurred in a "growing oxide core" manner with different nano-zones. The nano-range carbide particles did not show fragmentation or attrition as generally observed in micrometer range particles. Nevertheless, when the dimension of particles reached the micrometer range, the crystalline carbide phase appeared to be sprouted on the surface of magnetite single crystal.

In the previous reporting period, a design and operating philosophy was developed for an integrated wax filtration system for a 4 liter slurry bubble column reactor to be used in Phase II of this research program. During the current reporting period, we have started construction of the new filtration system and began modifications to the 4 liter slurry bubble column reactor (SBCR) reactor. The system will utilize a primary wax separation device followed by a Pall Accusep or Membralox ceramic cross-flow membrane. As of this writing, the unit is nearly complete except for the modification of a moyno-type pump; the pump was shipped to the manufacturer to install a special leak-free, high pressure seal.

TABLE OF CONTENTS

EXECUTIVE SUMMARY

In this reporting period, a fundamental filtration study to investigate the separation of Fischer-Tropsch Synthesis (FTS) liquids from iron-based catalyst particles was continued. Catalyst consumption due to filtration losses is a major expense in the operation of slurry phase FTS reactors using iron-based catalysts. Attrition of such catalysts in slurry-phase reactors produces a significant amount of fines, making catalyst separation from the products difficult. During slurry-phase FTS with bubble column reactors, catalysts are generally separated from accumulated reactor wax by either internal filtration or an external system which circulates catalyst back to the reactor. Catalyst fines produced by attrition may cause filters to plug and are difficult to separate by settling. As a result, multiple filtration stages are needed in order for the waxes to be well-suited for down-stream processing.

The overall objective of this filtration study is to test the effectiveness of various crossflow filtration procedures with simulant FTS slurry. The wax products from a FTS reactor can vary widely depending on the type of process implemented. In this study, the focus is on high-alpha iron-based slurry-phase reaction processes. The change in filtration properties of iron catalyst slurries will be correlated with physical and chemical changes of the particles during Fischer-Tropsch conditions.

In the current reporting period, the morphological and chemical nature of ultrafine iron catalyst particles (3-5 nm diameters) during activation/FTS was studied by HRTEM, EELS, and Mössbauer spectroscopy. The composition of the catalyst after 24 h CO activation was 85% $\chi - Fe_5C_2$ and rest magnetite. With the progress of FTS, the carbide re-oxidized to magnetite and catalyst activity gradually decreased. The growth of oxide phase continued and average particle size also increased simultaneously. The average particle size was 61.5 nm after 600 h of FTS. Some particles having maximum dimension larger than 130 nm was also observed. Amorphous carbon rims of 3-5 nm thickness around some of the particles and some hexagonal shaped particles were also observed. The thickness of carbon rims did not grow above 5-6 nm. Hence, the growth of particles was not due to carbon deposition on surface. The phase transformation occurred in a "growing oxide core" manner with different nano-zones. The nano-range carbide particles did not show fragmentation or attrition as generally observed in micrometer range particles. Nevertheless, when the dimension of particles reached the micrometer range, the crystalline carbide phase appeared to be sprouted on the surface of magnetite single crystal.

Work has begun to modify the CAER's 4 liter bubble column reactor to include the FT wax filtration scheme developed during the previous Phase of this research program. In the modified reactor system, a moyno-type progressive cavity pump will be included to convert the reactor from a natural to forced circulation liquid circuit. The wax/catalyst slurry will have two separate flow paths: 1. a low flow circuit (1-2 lpm) passing through the bubble column, and 2. a higher rate slurry path through the cross-flow filter.

TASK 1. Fundamental Filtration Studies

Task 1.1 Shakedown *(subtask completed)*

Task 1.2. Solvent wax experiments *(subtask completed)*

Task 1.3/1.5. Filtration studies with doping of olefins and alcohols and Development of Filter media cleaning procedure. *(subtask completed)*

Task 1.4. Ultra-fine Iron Filtration

Fischer-Tropsch Synthesis with Ultrafine Iron-Based Catalyst: Nano-Scale Growth of Particles

1. Introduction

Increasingly stringent environmental regulations for "clean-fuels" (low-sulfur, low-aromatics) make Fischer-Tropsch synthesis (FTS) an environmental-friendly route for production of middle-distillates and a wide variety of hydrocarbons and oxygenates from coal, natural-gas or biomass-derived synthesis gas (SG).[1] Iron-based catalysts are preferred for FTS utilizing a low H_2/CO ratio SG derived from coal or biomass because of their excellent activity in water gas shift reaction. The use of iron-based catalysts is also attractive in view of lower cost, lower methane selectivity, high olefin-selectivity, lower sensitivity towards poisons, and flexible product slate. When the operation favors long chain growth, a large amount of waxy material is produced that can be processed to produce premium fuels and chemical feed-stock. In removing wax, suspended particles must be separated and recycled back to the reactor to maintain required conversion and to avoid catalyst loss.[2] Catalyst/wax separation is also necessary for wax upgrading. The recommended solid content of the wax is 2-5 ppm.[2]

The use of iron catalysts in the most economical slurry bubble column reactors (SBCR) has been limited by their high rate of attrition to ultrafine particles leading to catalyst loss, high slurry viscosity and difficulty in wax/catalyst separation. Phase-transformations during activation/FTS play an important role in determining the structural integrity or attrition resistance of the catalyst particles. Sequential phase-modification during the activation process (with CO or SG) from hematite to magnetite

and finally to Fe_xC_y (iron carbides) have been reported.[3-6] The chemical conversion of Fe_3O_4 to Fe_xC_y induce a volumetric change due to significant difference in densities and resulting shear lead to formation of small crystallites of Fe_xC_y which split off rapidly to form ultrafine particles.[5,7-8] The conversion of Fe_3O_4 to Fe_xC_y is dynamic and reversible depending upon the environment. Under oxidizing conditions (e.g., at high water and CO_2 partial pressures), layers of surface Fe_3O_4 can form on carbide kernels and ultimately pure Fe_3O_4 crystals can be formed.[6] Thus the possibility of either fragmentation or growth of particles depending on the process condition exists. Kuo et al.[9] reported an increase in particle size during the slurry FTS which is contrary to what generally reported in literature. The particle size of most of catalysts used for attrition studies are in micrometer range. The use of submicron particles in SBCR is advantageous for efficient control and utilization of high reaction exotherm and enhanced mass transfer rate of gaseous reactants to catalyst surface. A detailed knowledge of the change of particle size of submicron particles is necessary for application in SBCR. The objective of the present study is to monitor the morphological and chemical change of ultrafine iron catalyst particles (3-5 nm diameters) during the activation/FTS in a CSTR by HRTEM, EELS, and Mössbauer spectroscopy. This information can be utilized for design and optimization of a filtration unit for wax separation.

2. Experimental

A commercial ultrafine iron oxide ($\alpha - Fe_2O_3$) catalyst (NANOCAT®, Mach I, Inc.; particle size, 3 nm; surface area, 250 $m^2\ g^{-1}$; bulk density, 0.05 g cm^{-3}) was used for all experiments. Polywax 850 (polyethylene fraction with average MW of 850) purchased from Baker Petrolite, Inc. was used as start-up solvent. Experiments were conducted in a CSTR equipped with a turbine impeller, a gas-inlet line, and a vapor outlet line with a fritted filter ($2\ \mu m$) placed external to the reactor. A tube fitted with a fritted filter ($0.5\ \mu m$) extends below the liquid level of the reactor maintains a constant level. A dip-tube was used to collect catalyst slurry at times. 54.7 g catalyst was added to 300 g melted (150 °C) Polywax 850. The temperature was raised to 270 °C at a rate of 1 °C min^{-1}. Catalyst was activated with CO at a SV of 3.0 sl h^{-1} g Fe^{-1} at 270 °C and 175 psig for 24 h. The FTS then started with a H_2/CO ratio of 0.7 and a SV of 3.0 sl h^{-1} g Fe^{-1}. The conversions were calculated from GC analysis of the exit gas. The products were collected in three traps maintained at 200, 100 and 0 °C and analyzed by GC. The slurry samples were diluted with hot (about 70 °C) o-xylene to remove the wax. Although it was not possible to completely remove the wax by this method, but the leftover wax did not interfere with TEM analysis and acted as a protective cover for the air-sensitive particles. An optimum ratio of o-xylene to catalyst was used to make a slightly turbid suspension for TEM analysis. A drop of the suspension was placed onto a lacey carbon film on 200 mesh copper grid and loaded into the microscope.

Mössbauer spectrums were collected in a transmission mode by a standard constant acceleration spectrometer (MS-1200, Ranger Scientific). A radiation source of 30 mCi ^{57}Co in Rh matrix was used and spectrums were obtained using a gas detector.

The solid catalyst slurry was mounted in plexiglass compression holders. Samples were investigated at room temperature as well as at cryogenic temperatures, typically over a velocity range of $\pm$ 10 mm s^{-1}. For the low temperature measurements, the samples were placed inside a vibration free closed cycle cryostat. The structural analysis of the samples was done by least-squares fitting using user defined functions within the PeakFit® program. Errors in the determined percent of Fe values are about $\pm$ 3-5 % depending on the complexity of the spectrums. The particle morphology was analyzed by a field emission analytical transmission electron microscope (JEOL JEM-2010F) operated at an accelerating voltage of 200 kV and equipped with a STEM unit with high-angle annular dark field (HAADF) detector, and a Gatan Imaging Filter (GIF)/PEELS system. The electron beam had a point-to-point resolution of 0.2 nm. EELS spectrums were recorded in TEM imaging mode with an energy resolution of 1 eV and dispersion rate of 0.2 eV/channel. Gatan Digital Micrograph® software was used for image and EELS data processing.

Table 1: The composition of the catalyst during the activation/FTS determined from Mössbauer spectroscopy. The CO activation (for 24 h) and FTS was carried out at 270 °C and 175 psig. The TOS was counted from the start of CO activation.

Sample # (TOS, h)	**Fraction (%) of Fe at 300 K**	**Fraction (%)of Fe at 20 K**
S1 (0 h)	85 in χ-Fe_5C_2 15 in spm	84 in χ-Fe_5C_2 16 in Fe_3O_4
S2 (28.9 h)	48 in χ-Fe_5C_2 33 in Fe_3O_4 19 in spm	50 in χ-Fe_5C_2 50 in Fe_3O_4
S3 (73.2 h)	65 in Fe_3O_4 18 in χ-Fe_5C_2 17 in spm	76 in Fe_3O_4 22 in χ-Fe_5C_2 2 in spm
S4 (167.7 h)	89 in Fe_3O_4 11 in spm	91 in Fe_3O_4 6 in χ-Fe_5C_2 3 in spm
S5 (311 h)	93 in Fe_3O_4 7 in spm	96 in Fe_3O_4 4 in spm

3. Results and Discussions

The initial activity of the ultrafine catalyst was high and showed a slow and gradual decrease during a total synthesis time of over 475 h (Figure 1). The removal of catalyst particles during the synthesis also accounts for the gradual decrease of conversion. Compositional changes in terms of percent peak area of the different iron species in Mössbauer spectrum are listed in Table 1. The superpara-magnetic (spm) phase

found at 300 K can be either Fe_3O_4 or iron carbide or a mixture of both phases. Hence, to identify the spm phase, the low temperature (20 K) results are considered. 24 h pretreatment with CO converts Fe_2O_3 to a mixture of 85% $\chi - Fe_5C_2$ and 15% magnetite which is in agreement with the reported results.[10] Low temperature Mössbauer results showed that the spm phase was magnetite, and not the iron carbide, which can also be present in spm phase.

The water produced in FTS acts as an oxidant and the oxidation of iron carbide continues with the synthesis time and the amount of carbide phase gradually decreases with a corresponding increase in fraction of magnetite phase. At the end of 311 h of synthesis time, the catalyst composes of mainly magnetite (96%) and the conversion of SG drops to a value lower than 15%. Thus the presence of some fraction of iron carbide is necessary for a catalyst to exhibit high activity in FTS.

Size analysis of irregular shaped particles requires some approximations of representative size. Non-equidimensional particles are often characterised by averaging major dimensions. Since, the particle sizes are measured from the TEM images, Feret diameter, the maximum distance between pairs of parallel tangents to the projected outline of the particle, is used. An arithmetic average of the first two large diameters (i.e., first two Feret diameter) has been taken as the "representative particle diameter" for the present study. The size of catalyst particles increased with the synthesis time. The FTS was started with an average particle size of 12.5 nm and after 620.8 h, the average particle size was 61.5 nm. Some particles with the largest dimension longer than 130 nm

was also observed (Figure 2a and 2b). Amorphous carbon rims of 3-5 nm thickness around some of the particles and some hexagonal shaped particles were observed. The bigger particles were formed during FTS (Figure 3). The variation of 'largest observed particle size' with TOS revealed a 10-fold increase of size. The thickness of carbon rims did not grow above 5-6 nm. Hence, the growth of particles is not due carbon deposition on surface.

TEM image of the fresh catalyst (Figure 4a) showed a particle size of (4-7) nm. The diffuse and non-sharp rings in the diffraction pattern (inset, Figure 4a) revealed the lack of well-defined crystallinity and inelastic scattering from ultrafine particles. The TEM image of samples activated in CO for 24 h showed a particle size in the range of 8-15 nm. The average diameter of the particles in this sample was 12.5 nm and a 2-3 nm rim of amorphous carbon around the some particles were visible. The diffraction pattern confirmed the presence of loose aggregates of iron carbides.[11] Carbide particles formed in layers overlapping with each other as found by HRTEM (Figure 4c & 4d). The carbides appeared as small crystallite with a d–spacing of 1.83 Å ([511] plane of Hägg carbide).

Crystallite with a d–spacing of 2.58 Å can be assigned either to the [311] plane of magnetite or $\chi - Fe_5C_2$ (2.65Å for [311] plane or 2.5 Å for [002] plane). Some of the crystalline aggregates were composed of an outer layer of iron carbide and an unreduced magnetite core (Figure 4d) with a characteristic d–spacing of 2.92 Å ([220] plane). The formation of such nano-zone was also observed with particles at higher TOS. In Figure 5a (112.6 h TOS), an outer-zone composed of magnetite (with a d–spacing of 2.58 Å for [311] plane) formed by re-oxidation of carbides and a carbide inner-zone (d–spacing of 1.83 Å, [511] plane). Similar feature was observed in Figure 5b. The formation of such

nano-zones suggests that the reduction and re-oxidation occurs in a diffusion controlled manner (i.e., a "growing oxide core" fashion).

It was reported that while using particles of 100-200 micron in size, the carbide phase forms as small nodules on the surface of the magnetite and the phase transformation proceeds slowly into the bulk.[4,6] The volumetric change during the oxide to carbide transformation results the sprouting of carbide buds/nodules on the surface of magnetite crystal. However, such phenomena were not observed with nanometer range particles. The carbides were identified as bulk phase with layers and sometimes with an oxide core. When the dimension of magnetite formed during FTS reaches the micrometer range, some of the carbide phase appears as nodules at top of the magnetite crystal. This was confirmed by the EELS analysis coupled with STEM imaging (Figure 6). The larger particle was pure oxide while the nodule was carbidic in nature. The nature of the carbon was analyzed with the high-energy loss portion of the EELS spectrum at the carbon K-edge. The differences between the spectra of crystalline and amorphous carbon are due to the relative intensity of carbon $1s \rightarrow \pi^*$ and $1s \rightarrow \sigma^*$ core-level transitions which provides a robust measure of the percentage sp^2-bonded carbon. The spectra of both ordered and disordered graphite show a sharp π^* peak followed by a higher energy σ^* peak.[12] The spectrum for amorphous carbon, however, only has a small π^* shoulder with a sloping σ* peak. The shape of present EELS spectrum suggests that the carbon phase was crystalline which was in agreement with Mössbauer measurements.

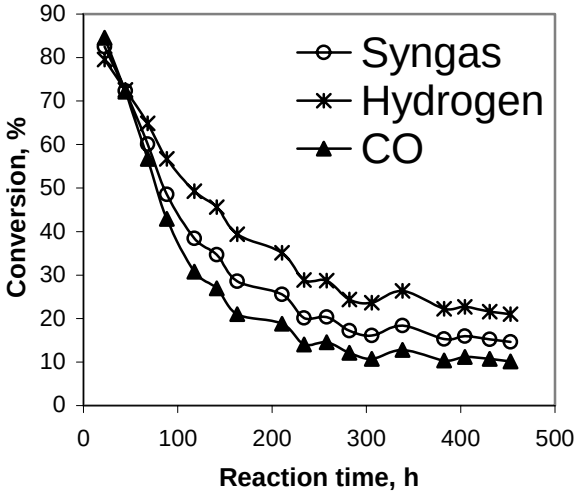

Figure 1: Plot of conversion of synthesis gas, H_2 and CO against time during the FTS (270 °C, 175 psig, 750 rpm) using iron nano-catalyst.

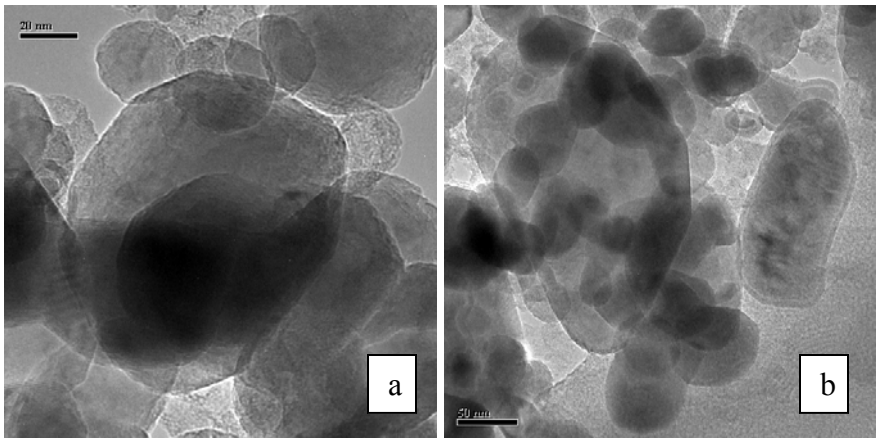

Figure 2: TEM image of particles after (a) 505.6 h & (b) 620.8 h TOS.

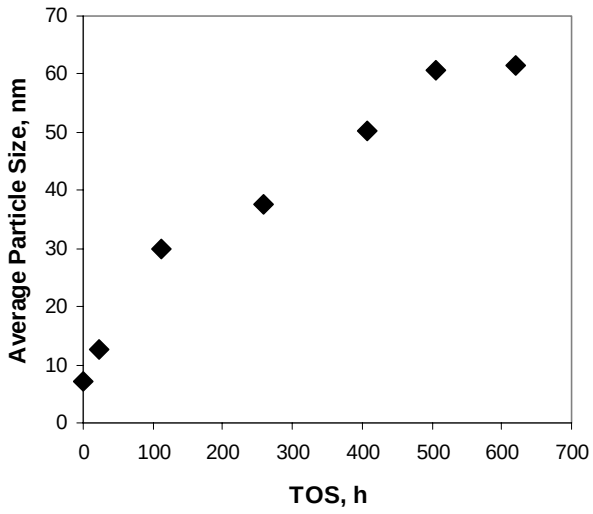

Figure 3: Variation of average particle size with TOS (counted from start of CO activation).

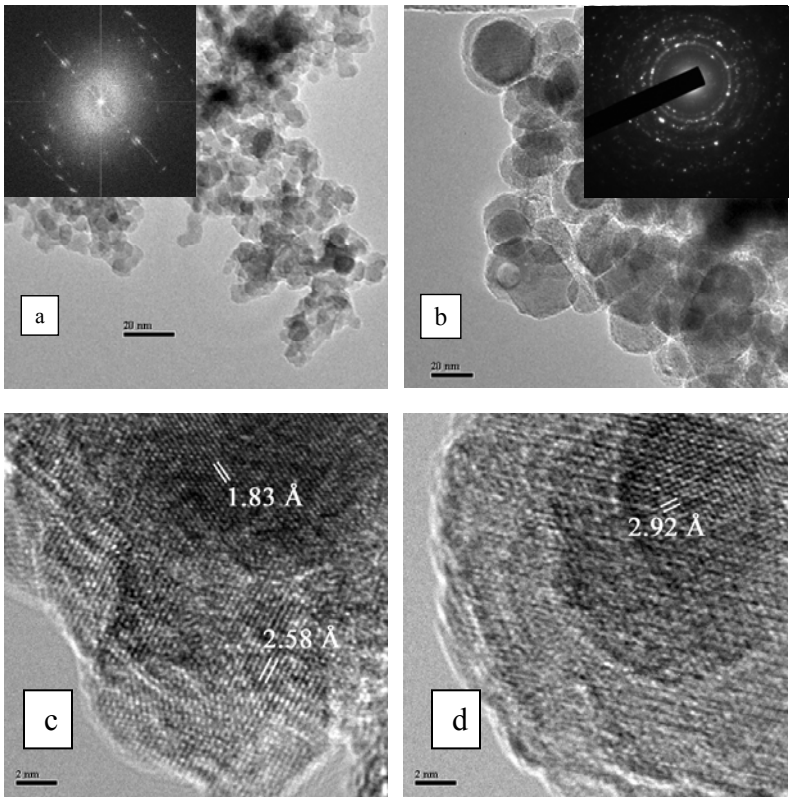

Figure 4: HRTEM image of particles: (a) fresh catalyst; (b, c, and d) CO activated (for 24 h) catalyst.

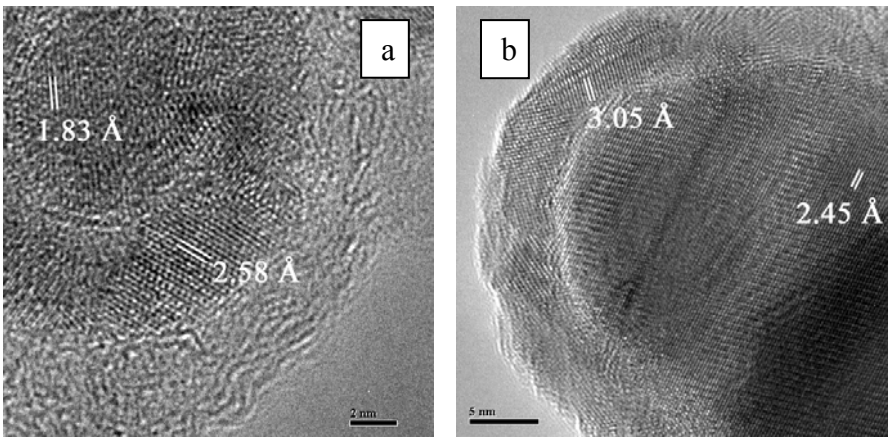

Figure 5: TEM image of particles after (a) 112.6 h; (b) 505.6 h TOS.

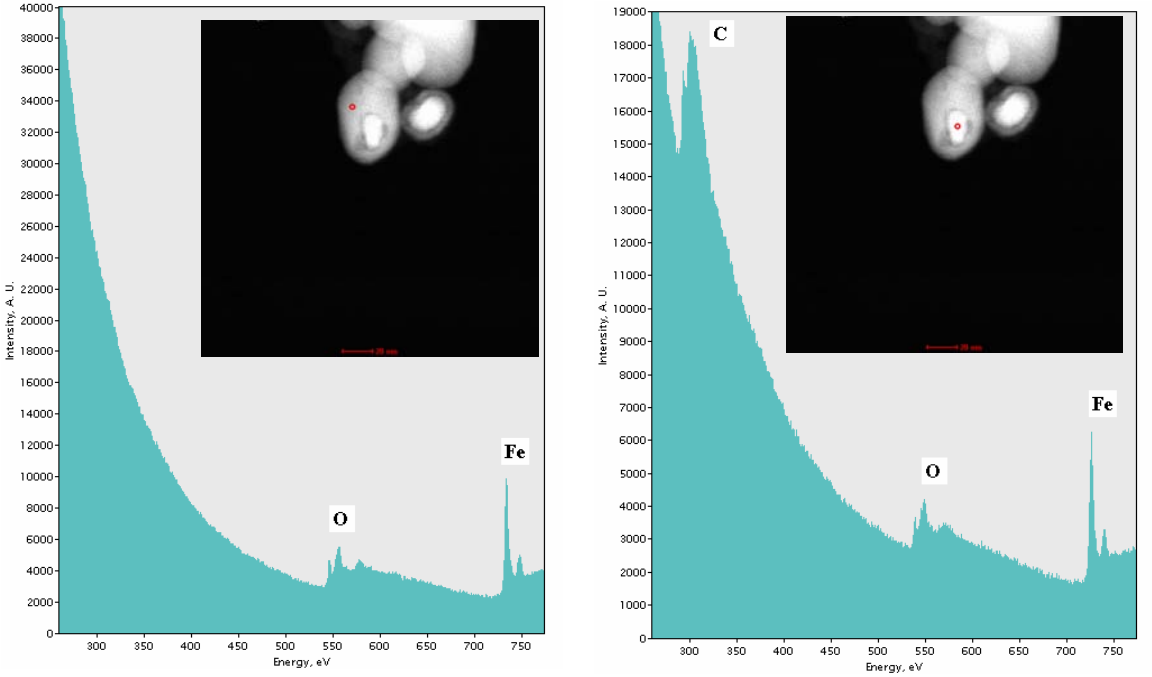

Figure 6: EELS spectrum of catalyst samples collected after 505.6 h TOS. Positions on the sample used to record the spectrum are also shown by high-resolution STEM (inset).

4. Conclusions

The change in size and morphology of ultrafine iron nano-catalyst during the FTS revealed a different phenomenon than commonly observed with micrometer sized iron catalysts. The phase transformation of ultrafine iron oxide to iron carbides does not create any fragmentation or attrition of the particles. This may be due to lower magnitude of stress generated (because of smaller size), by volumetric change in carbidation, and is not sufficient to break the particles. The small particles convert into carbides in a "shrinking core" manner with different nano-zones. The carbide/oxide conversions are dynamic and with the progress of FTS, the carbides get oxidized in a "growing oxide-core fashion" into pure single crystal oxide phase and grow in size. However, when the dimension of magnetite reaches in micrometer range, the crystalline carbide phase appears to be sprouted on the surface of magnetite single crystal.

5. References

1. Steynberg AP, and Dry ME, (eds), Fischer-Tropsch Technology, *Stud. Surf. Sc. Catal.*, 152, Elsevier, Inc.: San Diego, 2004.
2. Zhou PZ, and Srivastava RD, DOE Report, Burn and Roe Services (1991).
3. Huang CS, Ganguly B, Huffman GP, Huggins FE, and Davis BH, *Fuel Sc. Tech. Int'l*, 11 (9), 1289 (1993).
4. Shroff MD, Kalakkad DS, Coulte KE, Köhler SD, Harrington MS, Jackson NB, Sault AG, and Datye AK, *J. Catal.*, 156, 185 (1995).
5. Zhao R, Goodwin JG, Jothimurugesan K, Gangwal SK, and Spivey JJ, *Ind. Eng. Chem. Res.*, 40, 1320 (2001).
6. Li S, Ding W, Meitzner GD, and Iglesia E, *J. Phys. Chem. B*, 106, 85 (2002).
7. Srinivasan R, Xu L, Spicer RL, Tungate FL, and Davis BH, *Fuel Sci. Tech. Int'l*, 14(10), 1337 (1996).
8. Pham HN, and Datye AK, *Cata. Today*, 58, 233 (2000).
9. Kuo JCW, Sanzo FPD, Garwood WE, Gupte KM, Lang CK, Leib TM, Malladi M, Molina T, Nace DM, Smith J, Tarallo N, Kirk JF, DOE Report, Contract DE-AC22-83PC80019 (1985).
10. Rao KRPM, Huggins FE, Huffman GP, Gormley RJ, O'Brien RJ, and David BH, *Energy Fuels*, 10, 546 (1996).
11. Morozova OS, Maksimov YV, Shashkin DP, Shirjaev PA, Matveyev VV, Zhorin VA, and Krylov OV, *Appl. Catal.* , 78, 227 (1991).
12. Fernández A, Prieto P, Quirós C, Sanz JM, Martin JM, Vacher B, *Appl. Phys. Let.*, 69, 764 (1996).

Task 1.5. Development of Filter media cleaning procedure (CAER)

Subtask Completed.

Task 1.6. Chemical and physical characterization of slurry and filtrate

Abstract/Executive Summary:

The rate of initial carbidation, subsequent Fischer-Tropsch synthesis activity and catalytic stability of promoted iron-based catalysts are higher than the non-promoted catalysts. The objective of this research is to identify the role of alkali metal promoter using x-ray absorption spectroscopy technique.

X-ray Absorption Spectroscopy (XAS)

Sample Preparation:

Method: A commercial ultrafine iron oxide catalyst (NANOCAT® Superfine Iron Oxide, Mach I, Inc.) was promoted with rubidium carbonate (Sigma-Aldrich, Inc., 99.8%) and rubidium nitrate (Sigma-Aldrich, Inc., 99.7%) to get a final rubidium loading of 5 wt%. used for all experiments. Polywax 850 (polyethylene fraction with average molecular weight of 850) purchased from Baker Petrolite, Inc. was used as start-up solvent.

Methods: The FTS experiments were conducted in a 1 L CSTR equipped with a magnetically driven stirrer with turbine impeller, a gas-inlet line, and a vapor outlet line with a SS fritted filter (2 micron) placed external to the reactor. A tube fitted with a SS fritted filter (0.5 micron opening) extends below the liquid level of the reactor for withdrawing reactor wax (rewax) maintains a constant liquid level in the reactor. Another

SS dip-tube (1/8" OD) extends to the bottom of the reactor was used to withdraw catalyst/wax slurry from the reactor at times. Separate mass flow controllers were used to control the flow of hydrogen and carbon monoxide at the desired rate. The gases were premixed in a mixing vessel before entering to the reactor. Carbon monoxide was passed through a vessel containing lead oxide-alumina to remove any traces of iron carbonyl. The mixed gases entered the CSTR below the stirrer operated at 750 rpm. The reactor temperature was maintained ($\pm$ 1 °C) by a temperature controller.

54.7 g of iron oxide catalyst promoted with 5 wt% rubidium was added to melted (150 °C) Polywax 850 (300 g) in the CSTR to produce a slurry that contained about 15 wt% catalyst. The reactor temperature was then raised to 270 °C at a rate of 1 °C/min. The catalyst was activated using CO at a space velocity of 3.0 sl/h/g Fe at 270 °C and 175 psig for 24 h. At the end of activation a sample of activated catalyst-wax slurry (Sample S1) was withdrawn via the dip-tube at the end of activation period. The FTS was then started by adding synthesis gas mixture to the reactor at a space velocity of 3.0 sl/h/g Fe and a H_2/CO ratio of 0.7. The conversions of CO and H_2 were obtained by gas-chromatography analysis of the exit gas. The reaction products were collected in three traps maintained at different temperatures – a hot trap (200 °C), a warm trap (100 °C) and a cold trap (0 °C). The products were separated into different fractions (rewax, wax, oil and aqueous) for quantification. However, the oil and the wax fraction were mixed prior to GC analysis. Catalyst/rewax slurry was withdrawn at different reaction times via the dip-tube. The catalyst slurry coated with polywax 3000 and Fischer-Tropsch reactor was solidifies immediately at room temperature. The waxes acts as protective coating and prevents oxidation of catalysts.

X-ray Absorption Spectroscopy (XAS) Study

Beamtime has been arranged at beamline X-18b at the synchrotron at Brookhaven. Samples have been withdrawn from the reactor and stored under inert gas for testing. EXAFS tests will be carried out between June 16 - 19.

EXAFS is a technique that can provide information on the local atomic interactions. It has been proposed that the alkali plays an important role in promoting the formation of carbides. It is unknown precisely how the alkali operates in this function. It is not known, for example, whether K is present as isolated K^+ ions, whereby the electrons are donated to the catalyst surface (e.g., iron carbide surface) as in the jellium model [1] or whether the alkali is present in combination with other elements (e.g., K_2O or K_2CO_3 [2]). Addition of alkali or alkaline earth promoter has an important impact on shifting the product distribution toward heavier product [3], perhaps indicating an electronic effect. It has been suggested, for example, that the alkali enhances electronic back-donation to the $2\pi^*$ antibonding molecular orbitals of CO leads weakens the CO bond leading to an enhanced cleaving (i.e., dissociation) rate, thereby promoting the rate of carburization [4]. Recent density functional theory studies support this viewpoint [5].

Unfortunately, the K-edge of K lies at 3.6074 keV, which is below the allowable range for the beamline. Yet, the K-edge of rubidium Rb is 15.1997 keV, and is in the range. Since the promoting effect of alkali was found to be homologous for the group,

we have decided to investigate the local environment surrounding the element Rb by EXAFS.

In addition, the X-ray absorption near edge spectroscopy (XANES) region will provide electronic information on the state of the promoter. That is, the degree of electron transfer from the alkali promoter to the surface of the catalyst.

EXAFS and XANES measurements will also be used to assess the oxidation state and local structure surrounding the Fe absorber by analysis of the K-edge. Both analysis of the Rb and Fe K-edges will be carried out on a 5%Rb-promoted iron catalyst for each of the following conditions: (a) a fresh catalyst, (b) a catalyst sample withdrawn from the reactor after activation, and (c) samples withdrawn from the reactor during steady state FT testing.

1. J.W. Niemantsverdriet, Spectroscopy in Catalysis, VCH Verlagsgesellschaft 1993, Weinheim, Germany.
2. S. Li, G.D. Meitzner, E. Iglesia, J. Phys. Chem. B 105 (2001) 5743.
3. W. Ngantsoue-Hoc, Y-Q. Zhang, R.J. O'Brien, M-S. Luo, B.H. Davis, Appl. Catal. A 236 (2002) 77.
4. S. Jenkins, D.A. King, J. American Chemical Society 122 (2000) 10610-10614.
5. Z-P. Liu, P. Hu, Liu, Zhi-Pan; Hu, P. J. Am. Chem. Soc. 123 (2001) 12596.

Task 2. Phase II Bubble Column Pilot Plant Studies

INTRODUCTION

In the second phase of the current program, a pilot-scale SBCR system is to be integrated with a filtration scheme with procedures and equipment developed in Phase I. In Phase I, filtration properties of various iron-based catalyst slurries were correlated with the chemical and physical changes occurring during activation and FTS synthesis. Our research has focused on understanding of the phase changes during activation/reduction and their associated effects on filtration properties. Additionally, cleaning/flux maintenance procedures were optimized for the various filter media types test in the research program.

In the beginning of this research program, our objective was to develop a single-stage filtration scheme that would produce a wax with clarity of less the 5 ppm. Based on our operating experience and analytical information gathered with the pilot filtration rig in Phase I, this objective was overly optimistic in hindsight. A two-stage system is required because of the combined stresses of catalyst loading and the formation of nano-scale carbide particles formed during activation and synthesis. Additionally, the fouling rate of the filter media is directly proportional to catalyst slurry concentration; thus, a primary separation stage would have the potential to lower the stress on the filtration membrane.

In Phase II, our objective is to address the technical barriers associated with integrating an improved filtration strategy into commercial FTS unit. A series of pilot plant runs will obtain all the necessary data needed for the F-T filter system scale-up.

Laboratory evaluations will also be used to support the pilot tests help to optimize both the F-T catalyst and the overall process.

At present, work has begun to modify the CAER's 4 liter bubble column reactor to include the FT wax filtration scheme developed during the previous Phase of this research program. In the modified reactor system, a moyno-type progressive cavity pump will be included to convert the reactor from a natural to forced circulation liquid circuit. The wax/catalyst slurry will have two separate flow paths: 1. a low flow circuit (1-2 lpm) passing through the bubble column, and 2. a higher rate slurry path through the cross-flow filter.

EXPERIMENTAL

Integrated SBCR Two-StageFiltration Apparatus

In the current configuration, the bubble column has a 5.08 cm diameter and a 2 m height with an effective reactor volume of 3.7 liters; a simplified schematic of the SBCR system is shown in Figure 1. The synthesis gas passes continuously through the reactor and is distributed by a sparger near the bottom of the reactor vessel. The product gas and slurry exit the top of the reactor and pass through an overhead receiver vessel where the slurry was disengaged from the gas-phase. Vapor products and unreacted syngas exit the overhead separator vessel, enter a warm trap (333 K) followed by a cold trap (273 K) (see the photograph in Figure 2). A dry flow meter down stream of the cold trap measures the exit gas flow rate.

A downcomer tube, descending from the overhead separator, carries the F-T catalyst slurry to the suction side of a moyno-type progressive cavity pump. The slurry is

discharged from the pump to a primary separation device (an inertial separator similar to a hydroclone, see Figure 3). From the bottom of the primary separator, a catalyst-rich stream will be recycled to the reactor vessel while the lean catalyst/slurry stream will be diverted to a filtration circulation loop.

The flow rate of catalyst-rich slurry to the reactor will be controlled manually (1-3 lpm) by adjusting a throttle valve connected to the bottom of the primary separator such that the catalyst is well-dispersed in the SBCR. The filtration loop flow rate will be measured by a non-intrusive coriolis flow meter (see Figure 4). A detailed schematic of the filtration and reactor piping is shown in Figure 5. Quantifying the flow will be important because the slurry axial velocity is crucial in cross-flow filtration. The flow rate of slurry to the reactor will be measured indirectly by difference by temporarily cutting off the flow to the reactor and measuring the flow increase in the filtration loop. Since the slurry pump is a positive displacement device (i.e., no slurry slippage inside the pump), the total flow should remain the same regardless of pressure changes incurred by the temporary switching of the reactor circuit.

Polishing of the clarified slurry will be by a cross-flow filter element (eg, Aucusep or ceramic Membralox as shown in Figure 6), similar to the type supplied by Pall Filtration in Phase I. The filter assembly is configured such that the filter media could be replaced on-line, without aborting or interrupting the reactor run. The flux of the clean permeate through the cross-flow unit wax will be controlled by the pressure in the let-down vessel or hot trap. Therefore, the trans-membrane pressure (TMP) will be fixed for a given filtration event. The TMP can be changed manually varying the set

point of the pressure regulator connected to the let-down vessel. The flux rate is measured by weighing the mass of permeate collected in the collection vessel hot trap.

A filtration event is initiated by the overhead vessel level controller. The wax permeate flow from the filter will be switched on by a control valve between the permeate discharge of the cross-flow unit and the collection vessel. Hence, a relatively constant inventory of slurry will be maintained within the SBCR system as long as the superficial gas velocity remains constant. Changes in the gas hold-up due to a variable gas velocity will need to be calculated so that the space velocity can be accurately quantified.

The level or volume of the slurry within the overhead receiver is continuously monitored by measuring the differential pressure across the height of the vessel. Argon is purged through each of the pressure legs to keep the lines free of slurry. Slurry volume within the receiver is controlled to be no more than 1.3 liters by removing wax from the reactor system via the level control valve.

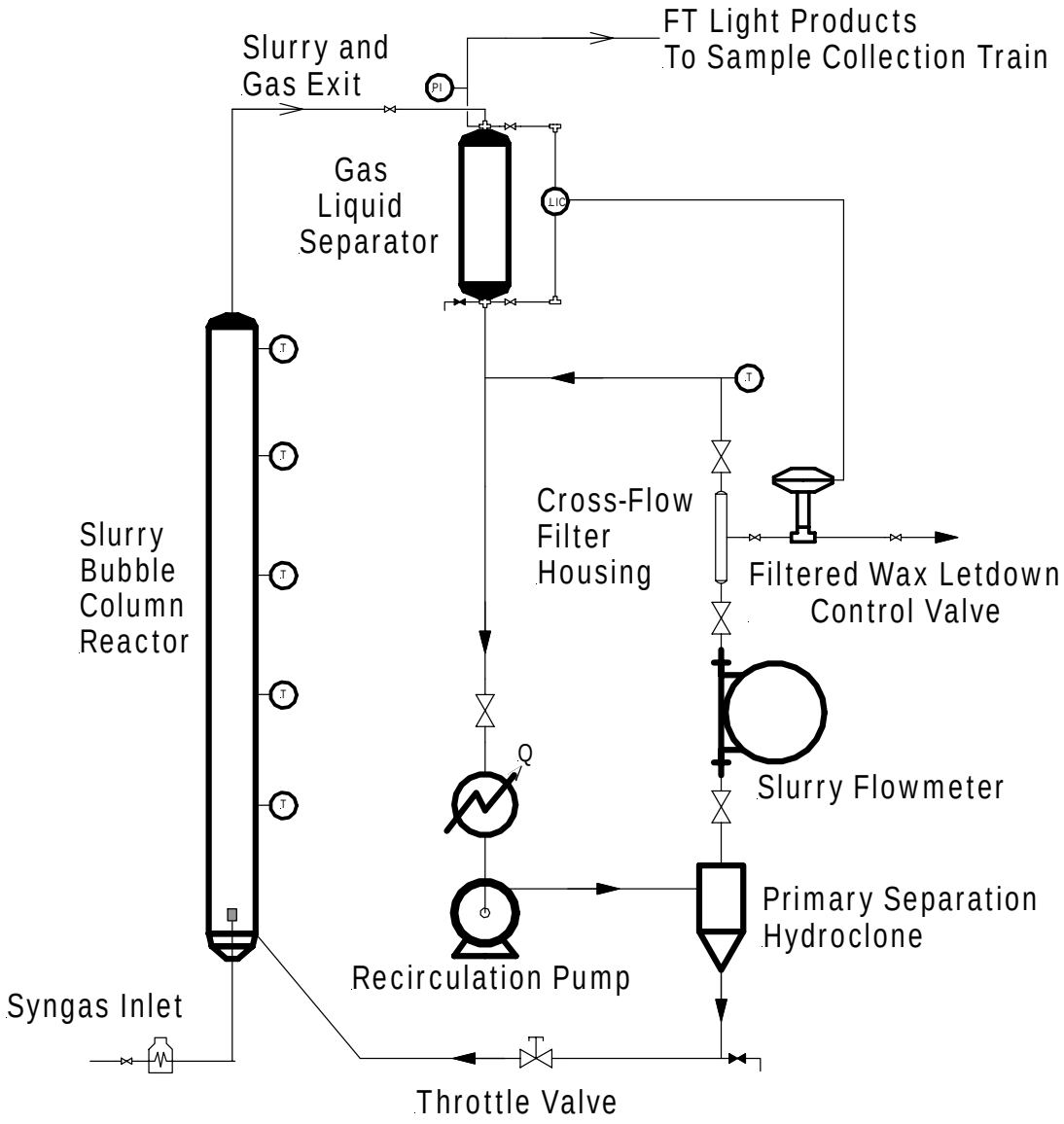

Figure 1. Simplified Schematic of Integrated SBCR/Filtration System

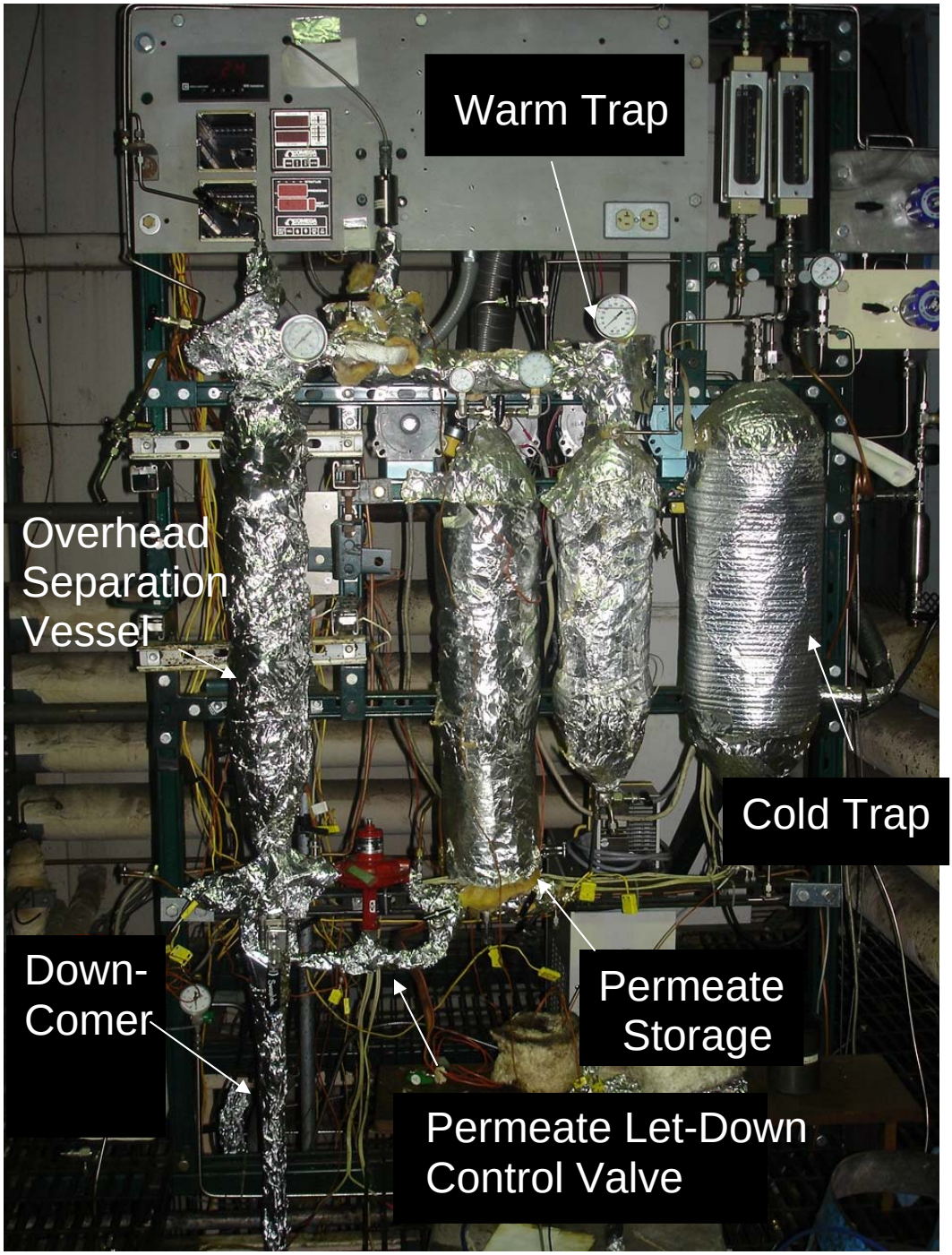

Figure 2. Overhead Receiver and Sample Traps.

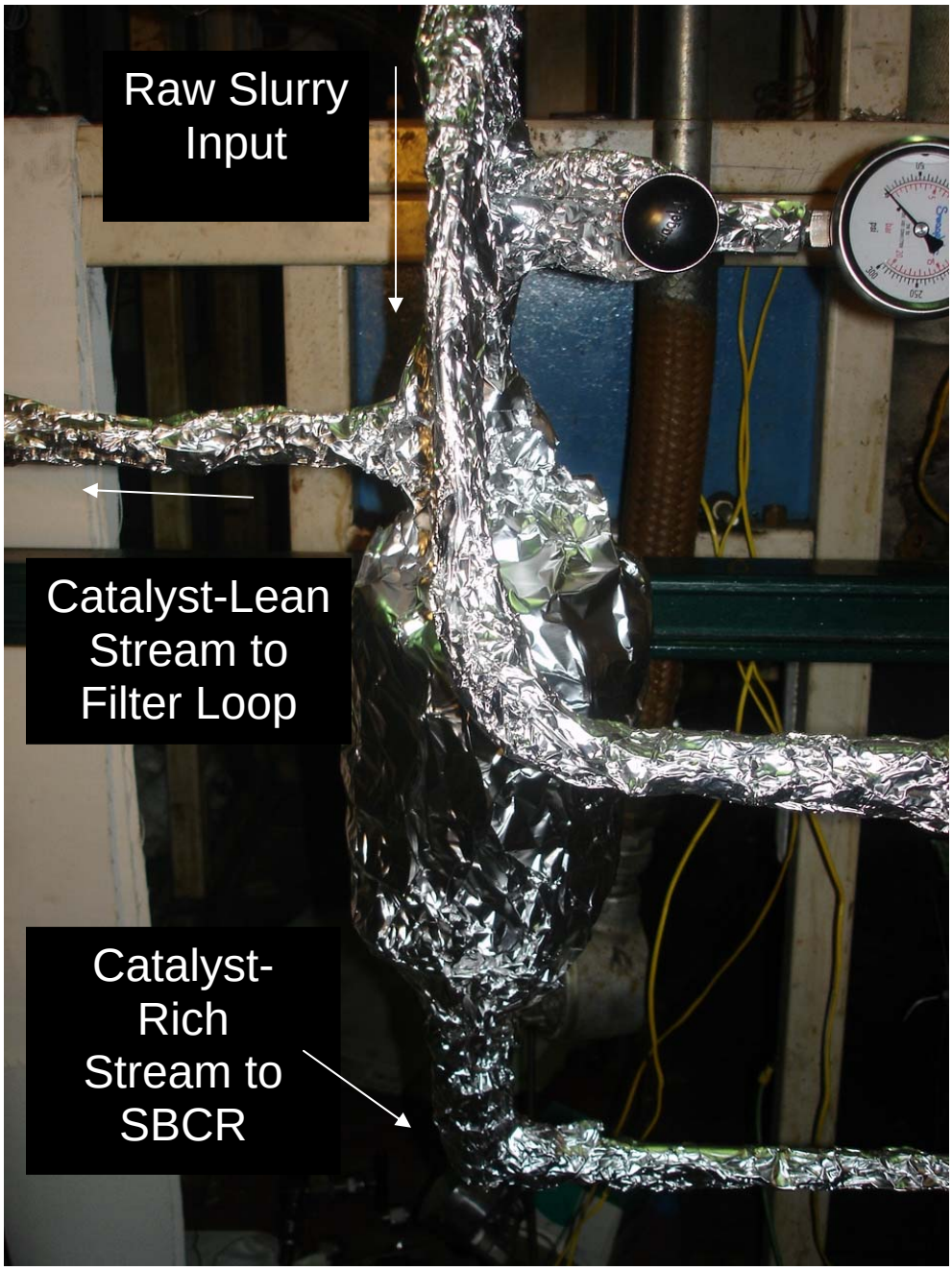

Figure 3. The Primary Separation Device.

Figure 4. The Newly Installed Slurry Flowmeter.

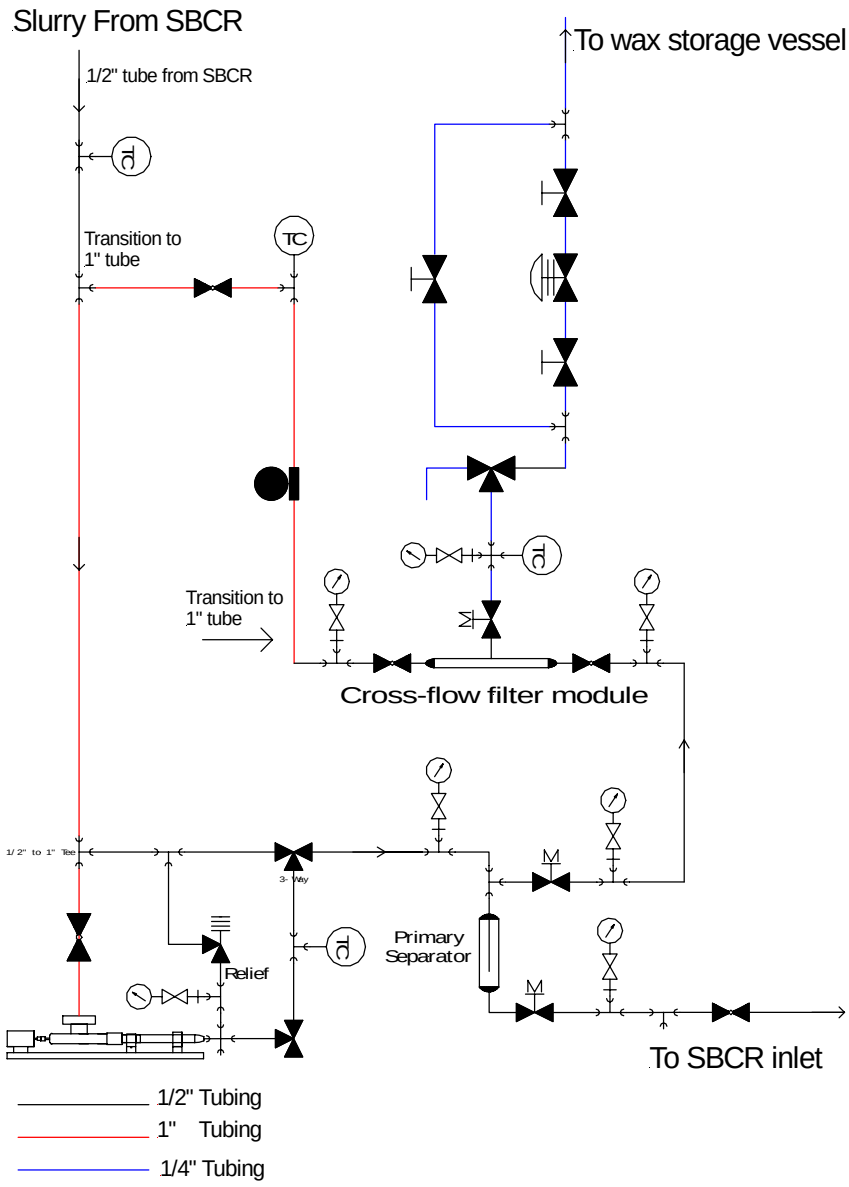

Figure 5. Piping Diagram Detail of the Filtration Loop.

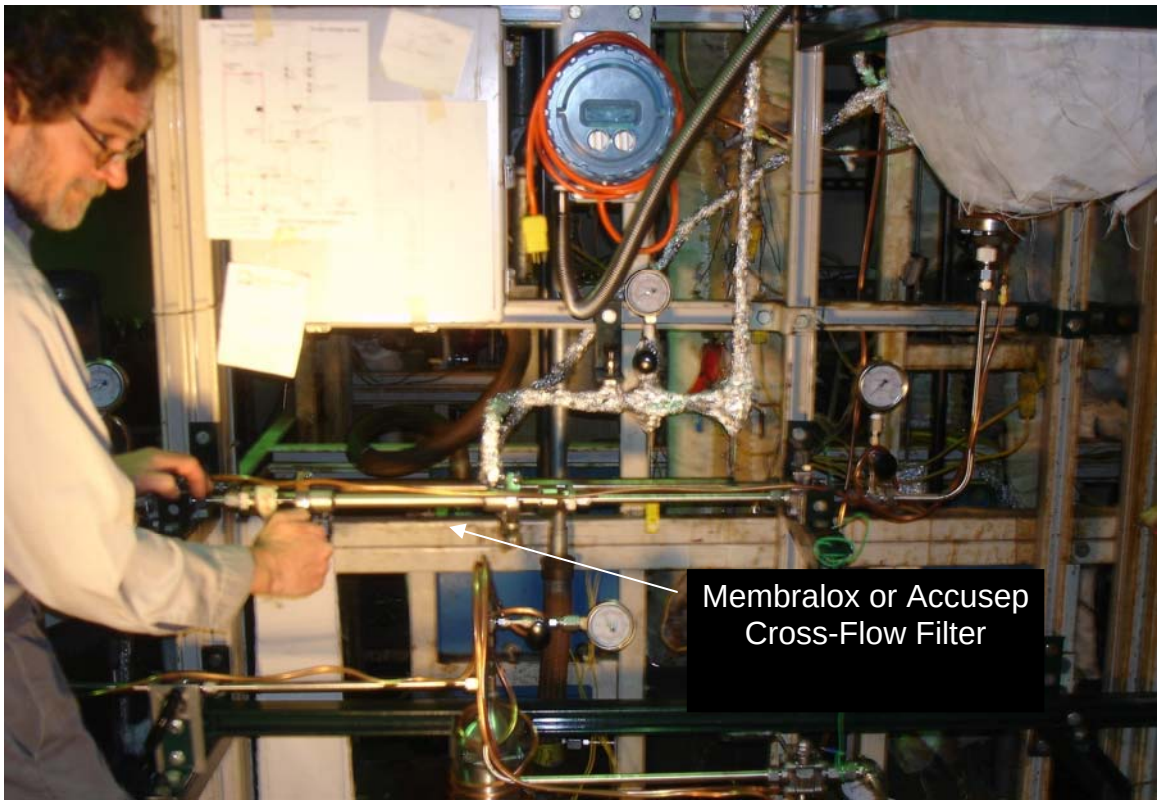

Figure 6. Installation of the Filter Tube Assembly.

CONCLUSIONS

The Phase I test program has provided the information and operational experience to integrate an improved filtration system for providing ultra-clean product wax. A series of pilot plant runs in Phase II will obtain all the necessary data needed for the F-T filter system scale-up. Modifications to SBCR to include the new filtration scheme are nearly complete. The slurry recirculation was shipped back to the manufacturer due to a problem with the high-pressure slurry seal.

PATENTS, PRESENTATIONS AND PUBLICATIONS

Patents Issued 2006

N/A

Papers published/accepted 2005 / 2006

1. Jacobs, G.; Graham, U.M.; Chenu, E.; Patterson, P.M., and Davis, B.H.; "Low temperature water-gas shift: impact of Pt promoter loading on the partial reduction of ceria, and consequences for catalyst design," Journal of Catalysis 229 (2005) 499.

2. Shi, B.; Jacobs, G.; Sparks, D.E.; and Davis, B.H.; "Fischer-Tropsch Synthesis: ^{14}C Labeled 1-alkene conversion using supercritical conditions with Co/Al_2O_3," Fuel 84 (2005) 1093.

3. Jacobs, G. and Davis, B.H.; "Reverse water-gas shift: steady state isotope switching study of the reverse water-gas shift reaction using in-situ DRIFTS over Pt/ceria," Applied Catalysis A: General 284 (2005) 31.

4. Chenu, E.; Jacobs, G.; Crawford, A.C.; Keogh, R.A.; Patterson, P.M.; Sparks, D.E.; and Davis, B.H.; "Water-gas Shift: an examination of unpromoted and Pt promoted MgO and tetragonal and monoclinic ZrO_2 by in-situ DRIFTS," Applied Catalysis B: Environmental 59 (2005) 45.

5. Jacobs, G.; Crawford, A.C.; Davis, B.H.; "Water-gas shift: steady state isotope switching study of the water-gas shift reaction using in-situ DRIFTS over Pt/ceria," Catalysis Letters 100 (2005) 147.

6. Jacobs, G. and Davis, B.H.; "In-situ DRIFTS investigation of the steam reforming of methanol over Pt/ceria," Applied Catalysis A: General 285 (2005) 43.

7. Das, T.K.; Jacobs, G.; and Davis, B.H.; "Deactivation of Promoted and Unpromoted Cobalt-alumina Catalysts," Catalysis Letters 101 (2005) 187.

8. Dalai, A.K.; Das, T.K.; Chaudhari, K.V.; Jacobs, G.; and Davis, B.H.; "Fischer-Tropsch synthesis: Water effects on Co supported on Wide and Narrow-pore silica," Applied Catalysis A: General 289 (2005) 135.

9. Jacobs, G.; Patterson, P.M.; Graham, U.M.; Crawford, A.C.; Davis, B.H.; "Low temperature water-gas shift: the link between the catalysis of WGS and formic acid decomposition over Pt/ceria," International Journal of Hydrogen Energy 30 (2005) 1265.

10. Jacobs, G.; Ricote, S.; Patterson, P.M.; Graham, U.M.; Dozier, A.; Khalid, S.; Rhodus, E.; and Davis, B.H.; "Low temperature water-gas shift: examining the efficiency

of Au as a promoter for ceria-based catalysts prepared by CVD of a Au precursor," Applied Catalysis A: General 292 (2005) 229.

11. Das, T.K.; Conner, W.A.; Li, J.; Jacobs, G.; Dry, M.E.; and Davis, B.H.; "Fischer-Tropsch Synthesis: Kinetics and Effect of Water for a Co/SiO_2 Catalyst," Energy & Fuels 19 (2005) 1430.

12. Jacobs, G.; Patterson, P.M.; Graham, U.M.; Crawford, A.C.; Dozier, A.; and Davis, B.H.; "Catalytic links among the water-gas shift, water-assisted formic acid decomposition, and methanol steam reforming reactions over Pt promoted thoria," Journal of Catalysis 235 (2005) 79.

13. Jacobs, G.; Ricote, S.; Graham, U.M.; Patterson, P.M., and Davis, B.H.; "Low temperature water gas shift: type and loading of metal impacts forward decomposition of pseudo-stabilized formate over metal/ceria catalysts," Catalysis Today 106 (2005) 259.

14. Jacobs, G.; Ricote, S.; and Davis, B.H.; "Low temperature water-gas shift: type and loading of metal impacts decomposition and hydrogen exchange rates of pseudo-stabilized formate over metal/ceria catalysts," Applied Catalysis A:General 302 (2006)14.

15. Sparks, D.E.; Patterson, P.M.; Jacobs, G.; Crocker, M.; and Chaney, J.A.; "Supported bismuth oxide catalysts for the selective reduction of NO with propene in lean conditions," Catalysis Communications 7 (2006) 122.

16. Ricote, S.; Jacobs, G.; Milling, M.; Ji, Y.; Patterson, P.M.; and Davis, B.H.; "Low temperature water-gas shift: characterization and testing of binary mixed oxides of ceria and zirconia promoted with Pt," Applied Catalysis A: General 303 (2006) 35.

17. Sparks, D.E.; Patterson, P.M.; Jacobs, G.; Dogimont, N.; Tackett, A.; Crocker, M.; "Bi_2O_3/Al_2O_3 catalysts for the selective reduction of NO with hydrocarbons in lean conditions," Applied Catalysis B: Environmental, *available online*.

18. Das, T.K.; Conner, W.A.; Jacobs, G.; Zhan, X.; Li, J.; Dry, M.E.; and Davis, B.H.; "Fischer-Tropsch Synthesis: Kinetics and Effect of Water for a Co/Al_2O_3 Catalyst," book chapter, accepted, in press.

19. Jacobs, G.; Das, T.K.; Li, J.; Luo, M.; Patterson, P.M.; and Davis, B.H., "Fischer-Tropsch synthesis: influence of support on the impact of co-fed water for cobalt-based catalysts," book chapter, accepted, in press.

Papers submitted/submitting/under review 2006

1. Jacobs, G.; Keogh, R.A.; Davis, B.H., "Hydrogen production catalysis: conversion of ethanol and acetic acid by steam over Pt/ceria, *submitted*.

2. Jacobs, G.; Ricote, S.; and Davis, B.H.; "Low temperature water-gas-shift reaction: interactions of steam and CO with ceria treated with different oxidizing and reducing environments," *submitting*.

3. Jacobs, G.; Milling, M.; Ji, Y.; Patterson, P.M., Sparks, D.E., and Davis, B.H., "Characterizing mixing in solid solutions of $Hf_XZr_{1-X}O_2$ by EXAFS applying a simultaneous fitting model to Hf L_{III} and Zr K edge data - relationship between bulk and surface composition, and impact on catalytic selectivity for dehydration versus dehydrogenation of alcohols," *submitting*.

Presentations and Symposia 2005/2006

1. Jacobs, G.; Das, T.K., Li, J., Luo, M.; Patterson, P.M., and Davis, B.H.; "Fischer Tropsch synthesis: Influence of support on the impact of water for cobalt-based catalysts," Abstracts of Papers, 229th ACS, Div. Petr. Chem., National Meeting, San Diego, CA, United States, March 13-17, 2005 (2005).

2. Crocker, M.; Graham. U.; Gonzalez, R.; Morris, E.; Jacobs, G.; Andrews, R. "Preparation and characterization of fibrous cerium oxide templated from activated carbon fibers," 2005 Materials Research Society Spring Meeting, Mar. 28 - Apr. 1, San Francisco, CA, 2005.

3. Patterson, P.M.; Sparks, D.E.; Jacobs, G.; Dogimont, N.; Tackett, A.; Crocker, M.; "Development of New Catalysts for NO_X Emission Control Based on Bismuth Oxide," 3rd Annual Kentucky Innovation & Enterprise Conference, Mar. 31, Louisville, KY, 2005.

4. Jacobs, G.; Patterson, P.M.; Crawford, A.C.; and Davis, B.H.; "Developing Structural Property Relationships of Pt/Ceria Catalysts for Low Temperature Water Gas Shift,"Atlanta, GA, AICHE Spring National Meeting, April 10-14, 2005.

5. Davis, B.H.; Das, T.K.; Chaudhari, K.; Jacobs, G.; and Luo, M.; "Impact of Water on Iron and Cobalt Catalysts During Synthesis,"Atlanta, GA, AICHE Spring National Meeting, April 10-14, 2005.

6. Patterson, P.M.; Sparks, D.E.; Jacobs, G.; Tackett, A.; Chaney, J.A.; and Crocker, M.; "Supported Bismuth Oxide Catalysts for NO_X Reduction Using Hydrocarbon Reductants," 19th North American Meeting of The Catalysis Society, May 22-27, Philadelphia, PA 2005.

7. Jacobs, G.; Patterson, P.M.; and Davis, B.H.; "Low Temperature Water-Gas Shift: Isotopic Tracer and Kinetic Isotope Effect Investigations Over Pt/ceria,"19th North American Meeting of The Catalysis Society, May 22-27, Philadelphia, PA 2005.

8. Jacobs, G.; Ricote, S.; Graham, U.M.; Patterson, P.M.; and Davis, B.H., "Low

temperature water gas shift: type and loading of metal impacts forward decomposition of pseudo-stabilized formate over metal/ceria catalysts", International Conference on Gas-Fuel, November 13-16, Brugge, Belgium 2005.

9. Jacobs, G.; Das, T.K.; Li, J; Patterson, P.M.; Luo, M.; Davis, B.H. "Fischer-Tropsch Synthesis: Impact of water on the activity and lifetime of cobalt catalysts," 10th International Symposium on Catalyst Deactivation, Feb 3-7, Berlin, Germany, 2006.

10. Jacobs, G.; Ricote, S.; Ji, Y.; Patterson, P.M., Davis, B.H., "Metal Promoted Binary Oxides of Ceria and Zirconia for Low Temperature Water-Gas Shift", AICHE Spring National Meeting, April 23-27, 2006.

11. Luo, M., Jacobs, G., and Davis, B.H., "Overview of Fischer-Tropsch Products and Their Upgrading to Useful Products.", AICHE Spring National Meeting, April 23-27, 2006.

12. Amitava Sarkar, U. Graham, J. K. Neathery, R. L. Spicer, and B. H. Davis, Fischer-Tropsch Synthesis with Ultrafine Iron-Based Catalyst: Nano-Scale Growth of Particles and Associated Effects on Wax/Catalyst Separation, A IChE Spring National Meeting, April 23-27, 2006, Orlando, USA.

13. Amitava Sarkar, U. Graham, J. K. Neathery, R. L. Spicer, and B. H. Davis, Nano-scale growth of iron-based catalysts in Fischer-Tropsch Synthesis, 231 st ACS National Meeting, March 26-30, 2006, Atlanta, USA.

TRAVEL